Article

Solid Particle Mobility in Agitated Bingham Liquids

J. J. Derksen

Ind. Eng. Chem. Res., **2009**, 48 (4), 2266-2274• DOI: 10.1021/ie801296q • Publication Date (Web): 15 January 2009

Solid Particle Mobility in Agitated Bingham Liquids

J. J. Derksen*

Chemical & Materials Engineering Department, University of Alberta, Edmonton, Alberta, T6G 2G6 Canada

Motivated by applications in oil sands processing, numerical simulations of the combined flow of yield-stress (Bingham) liquids and solid particles in a mixing tank have been performed. The conditions were such that, generally, the flow systems were in a transitional regime, between laminar and developed turbulence. The fluid flow was simulated according to a lattice-Boltzmann scheme, with the yield stress being mimicked as a highly viscous fluid for low deformation rates. Particles were assumed to move under the influence of drag, gravity, and particle−wall and particle−particle collisions. Agitation formed a cavity (active volume) around the impeller, with the rest of the tank being virtually inactive. This mobilized the particles in the cavity. In their ability to suspend and mobilize particles, agitated Bingham liquids behave markedly different from Newtonian liquids.

Introduction

Solid particles dispersed in continuous-phase liquids are practically relevant and intriguing systems. In industry, they are encountered in a wide variety of process equipment such as slurry reactors, crystallizers, polymerization reactors, transport pipelines, and liquid-fluidized beds. The momentum, energy, and mass transfer between the phases (e.g., hydrodynamic forces on particles) and within the phases [e.g., collisions between solid particles, (turbulent) stresses in the liquid] determine the distribution of the solids in the liquid, the relative velocity of the phases, and (as a consequence) the performance of the process. Solids interacting with small-scale turbulence give rise to preferential concentrations to an extent related to particle sizes and time scales relative to eddy sizes and eddy lifetimes.

In a large number of practical cases, the continuous phase behaves as a non-Newtonian fluid. Such behavior contributes significantly to the complexity of the multiphase system. Prominent applications of solid−liquid suspensions with non-Newtonian rheology of the liquid phase are found in oil sands processing. The separation of the bitumen (oil) phase from the solids (sands) phase involves the use of hot water, which tends to activate the clay contained in the oil sands. The activated clay particles form networks that provide the oil−water−solids mixture with a yield stress. This yield-stress (loosely termed Bingham-type) behavior of the mixture has consequences for the design, operation, and efficiency of oil sands processing, more specifically in those parts of the process related to separation and to tailings (where tailings are the process residuals; see Masliyah et al.[1] for an overview of oil sands processing). The clay network can hinder gravity-based separation: if net gravity is not strong enough to break through the yield stress, sand particles and/or bitumen droplets become immobilized. The consistency of the tailings depends largely on the strength of the clay network. In land reclamation at the end of the oil sands mining cycle, the tailings consistency is a crucial variable.

To reveal some of the above-mentioned solid−liquid interactions and to investigate whether and to what extent solid−liquid mixtures involving yield-stress liquids become mobilized by agitation, we performed a computational study. Bingham liquids loaded with solid particles of spherical shape were agitated in a mixing tank. The small (laboratory-scale) size of the tank and the relatively high (apparent) viscosity of the working liquid allowed for direct simulations of the liquid flow, i.e., the liquid flow could be fully resolved, without the need to apply (some sort of) turbulence modeling. The solid particles were simulated as "point particles" in a manner similar to (but simpler than) that discussed earlier by Derksen.[2] The notion of point particles implies that we do not directly resolve the flow around the individual particles (the particle diameter is smaller than the grid spacing of the liquid flow simulation). In the simulations, the dynamics of the solid particles is governed by the hydrodynamic forces (most notably drag) acting on them, which are determined from single-particle correlations based on particle-related Reynolds numbers. In addition to hydrodynamic forces, the solid particles feel net gravity; they collide with the vessel wall and vessel internals; and they mutually collide at a distance equal to $(d_{p1} + d_{p2})/2$, where d_{p1} and d_{p2} are the diameters of the particles involved in the collision.

To place the present study in an oil-sands-engineering perspective, it should be noted that the oil sands process streams are intrinsically multiscale. A rough distinction in phases counts up to four: a bitumen phase, a clay phase (small, surface-active solid particles), a sands phase (larger, inert particles), and the water phase. In the present study, we do not account for the oil phase. Further, we lump the clay−water mixture into a single phase with non-Newtonian rheology. The sand particles are treated explicitly, i.e., they are tracked as solid spheres through the non-Newtonian liquid phase in a Lagrangian manner.

In this initial study, we used a simplified liquid rheology. Specifically, we considered a time-independent Bingham liquid characterized by two parameters: a yield stress τ_0 and a viscosity η. In one-dimensional shear flow we defined the latter as the (constant) slope of the shear rate versus shear stress curve. In oil sands processing, the actual rheology of the liquid phase is more complicated because of the time-dependent (thixotropic) nature of the clay network. Fluid deformation will temporarily disintegrate the network; if deformation stops, the network needs time to build up.

This article is organized as follows: First, the flow system is defined in terms of its geometry and its dimensionless numbers. The representation of the Bingham liquid is explained, along with the assumptions made in simulating the solid particle motion. In presenting the results, the liquid flow field is characterized including the concept of an active volume and an essentially inactive volume. Also, the solid particles concentra-

* E-mail: jos@ualberta.ca.

10.1021/ie801296q CCC: $40.75
Published on Web 01/15/2009

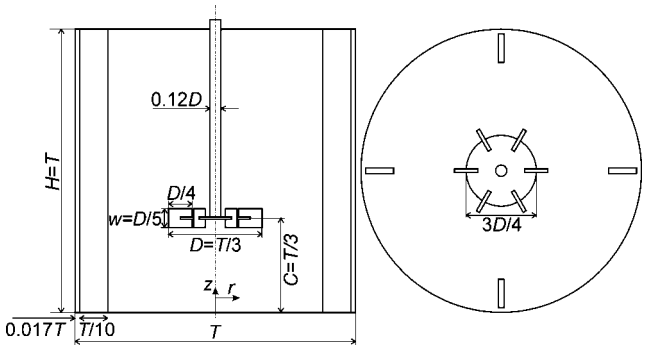

Figure 1. Stirred-tank geometry and (r,z) coordinate system. Left, side view; right, top view. The vessel content is covered with a lid (no-slip wall). The thickness of the impeller blades and disk amounts to $0.035D$; the thickness of the baffles amounts to $0.02T$. In this figure, the impeller clearance is $C = T/3$. Clearances of $T/4$ and $T/2$ have also been considered.

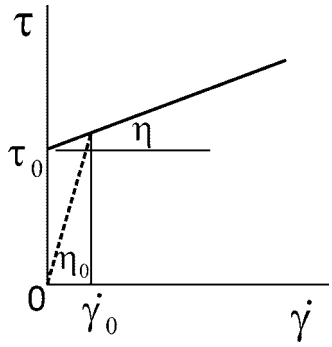

Figure 2. Schematic of Bingham rheology and its implementation in a viscous flow code. Solid line, actual rheology with parameters τ_0 and η; dotted line, for $\dot{\gamma} < \dot{\gamma}_0 \equiv \tau_0/(\eta_0 - \eta)$, the dotted line with slope η_0 is followed in the simulations.

tion and the solids velocity fields are presented. The conclusions and an outlook are given at the end of the article, along with a plea for modeling the complex systems at hand at multiple scales in order to capture the essential physical interactions.

Flow System and Liquids

In the system under investigation, the flow is generated by an impeller revolving in a mixing tank. The geometry of the tank and impeller are shown in Figure 1, along with a definition of the coordinate system employed. The impeller, a Rushton turbine, is a standard impeller in mixing research. All tank and impeller dimensions can be derived from the tank diameter T (see Figure 1). We used specifically this configuration because it allows for a comparison of our Bingham liquid results with a large body of data for Newtonian liquids and liquid−solid mixtures agitated in similar tanks.

The Bingham liquid is defined in terms of its yield stress, τ_0, and its viscosity, η (see Figure 2). In three-dimensional flow, the shear rate $\dot{\gamma}$ is generalized according to $\dot{\gamma} = (2d_{ij}d_{ij})^{1/2}$ (summation over repeated indices), with $d_{ij} = {}^1/_2(\partial u_j/\partial x_i + \partial u_i/\partial x_j)$ being the rate of strain tensor (where $\mathbf{u}$ is the fluid velocity vector). The Bingham model then reads

$$\tau_{ij} = 2\left(\frac{\tau_0}{\dot{\gamma}} + \eta\right)d_{ij} \quad \text{if } |\tau| > \tau_0$$
$$d_{ij} = 0 \quad \text{if } |\tau| \le \tau_0 \tag{1}$$

with $|\tau| \equiv ({}^1/_2\tau_{ij}\tau_{ij})^{1/2}$. The factor $(\tau_0/\dot{\gamma} + \eta)$ in eq 1 is often termed the apparent viscosity, η_a.

Once the flow geometry is specified, assuming that the working fluid is Newtonian with a density ρ and a dynamic viscosity η, the Reynolds number (traditionally defined as $Re = \rho ND^2/\eta$, where N is the impeller speed in revolutions per second) fully determines the flow. For Reynolds numbers below 10^2, the flow is laminar (albeit time-dependent because of the impeller rotating relative to the baffled tank wall); for $Re > 10^3$, the flow is considered turbulent; and for values between these limits, there is a transitional range. In the case of a Bingham liquid, we retain the above definition of the Reynolds number, with η as defined in eq 1 and Figure 2. Given the two-parameter rheological model that we use, a second dimensionless number comes into play. In this work, it has been defined as the yield stress relative to inertial stresses

$$Y \equiv \frac{\tau_0}{\rho N^2 D^2} \tag{2}$$

We prefer using Y as defined in eq 2 instead of the more commonly used Bingham number (see, e.g., Yu and Wachs[3]). The Bingham number represents yield stress relative to viscous stress; given the inertia-dominated nature of the flows that we anticipate, we prefer relating yield stress to inertia.

In this work, the lattice-Boltzmann method[4,5] was used for solving the flow equations. This method allows for the simulation of flows with varying viscosity (as is done, for example, in large-eddy simulations[6]). Bingham rheology was incorporated into the lattice-Boltzmann method by assuming that, at very low deformation rates, the fluid behaves as a very (though not infinitely) viscous fluid.[7] This introduces an additional (numerical) parameter η_0. At a critical deformation rate $\dot{\gamma}_0$ that is related to η_0 and the physical properties τ_0 and η $[\dot{\gamma}_0 \equiv \tau_0/(\eta_0 - \eta)]$ the fluid switches from slope η_0 to slope η in the deformation rate versus stress curve (see Figure 2).

The implementation of Bingham rheology in a lattice-Boltzmann scheme was tested by performing one-dimensional (laminar) planar channel flow simulations and comparing the results to the analytical solution. The velocity profiles as presented in Figure 3 indicate that, as long as $\eta_0 \ge 100\eta$, the region with $|\tau| < \tau_0$ hardly deforms, Bingham behavior is indeed observed, and the dependence on the (artificial) parameter η_0 is small.

Particles and Particle Dynamics Modeling

The solid particles that are released in the agitated Bingham liquid are considered to be monodisperse and spherical with diameter d_p and solid material density ρ_s. The motion of each individual particle is solved according to its equations of motion

$$\frac{\mathrm{d}\mathbf{x}_p}{\mathrm{d}t} = \mathbf{v}_p \quad \text{and} \quad \rho_s \frac{\pi}{6} {d_p}^3 \frac{\mathrm{d}\mathbf{v}_p}{\mathrm{d}t} = \sum \mathbf{F} \tag{3}$$

where $\mathbf{x}_p$ is the particle position vector and $\mathbf{v}_p$ is the particle velocity vector. The forces acting on the particle that are being considered are net gravity $\mathbf{F}_g$, drag $\mathbf{F}_D$, and the added-mass force $\mathbf{F}_{AM}$. These forces are defined as follows:

$$\mathbf{F}_g = (\rho_s - \rho)\frac{\pi}{6} {d_p}^3 \mathbf{g}$$

where $\mathbf{g}$ is gravitational acceleration, here pointing in the negative z direction

$$\mathbf{F}_D = C_D \frac{\pi}{4} {d_p}^2 \frac{1}{2} \rho |\mathbf{u} - \mathbf{v}_p|(\mathbf{u} - \mathbf{v}_p)$$

where C_D is the drag coefficient and $\mathbf{u}$ is the fluid velocity at the position of the particle

$$\mathbf{F}_{AM} = \frac{1}{2}\rho\frac{\pi}{6}{d_p}^3\frac{d\mathbf{v}_p}{dt}$$

The drag coefficient, C_D depends on the Reynolds number based on the slip velocity of the particle and the apparent viscosity at the position of the particle [$Re_p = (\rho|\mathbf{u} - \mathbf{v}_p|d_p)/\eta_a$] according to the Schiller and Naumann[8] correlation

$$C_D = \frac{24}{Re_p}(1 + 0.15{Re_p}^{0.687})$$

Applying this correlation to particles moving through non-Newtonian liquids is a simplification that requires further investigation. However, numerical simulations by Yu and Wachs[3] demonstrated a clear correlation between the drag coefficient and the Reynolds number based on the apparent viscosity with flow structures around the sphere reminiscent of Newtonian flow. Also, for reasons of simplicity, and because we expect drag to be the dominant hydrodynamic force under the relatively viscous (low-Re_p) conditions, we neglected history, lift, and stress-gradient forces. We also did not consider particle rotation.

Equation 3 is solved simultaneously with the flow equations; it is discretized according to an Euler implicit scheme with a time step equal to the time step with which the flow field is being updated.

In the liquid−solid suspensions considered here, we expect a significant influence of particle−particle and particle−wall collisions on the solid particle dynamics. In a previous work,[2] it was demonstrated that the excluded-volume effect as a consequence of particle−particle collisions was necessary for correctly describing vertical solids concentration profiles in agitated Newtonian suspensions. In the present study, hard-sphere collisions are explicitly resolved according to the time-step-driven algorithm developed by Chen et al.[9] For computational reasons, this collision algorithm considers at most one collision per time step per particle. This approach works well for the semidilute cases as considered here.[2]

In most of the simulations, the solid particles are one-way-coupled to the liquid; that is, the particles feel and are moved by the liquid, but the hydrodynamic forces are not fed back to the liquid flow dynamics. This assumption will be assessed by incidentally comparing results of one-way-coupled simulations with those of two-way-coupled simulations. In the two-way-coupled simulations, we used the particle-source-in-cell (PSIC) approach;[10] the drag force on a particle is fed back to the fluid phase as a momentum source that is linearly distributed over the eight lattice nodes surrounding the particle.

Characteristics of Flow Cases

We simulate laboratory-scale systems with a tank volume of 10 L and liquid properties that relate to oil sands (tailings) practice: $\tau_0 = 10$ N/m^2, $\eta = 10^{-2}$ Pa·s, $\rho = 10^3$ kg/m^3. A 10-L tank with the geometrical layout shown in Figure 1 has a diameter $T = 0.234$ m. The impeller diameter is $D = T/3 = 0.078$ m (see Figure 1). In the base case, the impeller spins with $N = 10$ revolutions per second; as a consequence $Re = 6 \times 10^3$ and $Y = 1.64 \times 10^{-2}$. Based on these numbers, we anticipate mildly turbulent flow conditions, at least in the region close to the impeller where the apparent viscosity is expected to approach η.

The solid particles as used in the base case have a diameter of $d_p = 0.65$ mm ($= 0.0083D$) and a density of $\rho_s = 2.5 \times 10^3$ kg/m^3. At the base-case solids mass fraction of $\phi_m = 0.0337$ (achieved by inserting 942 569 spheres into the tank), such particles immersed in the same tank filled with fluid of the same viscosity ($\eta = 10^{-2}$ Pa·s) but without a yield stress would need an impeller speed of $N_{js} = 25$ revolutions per second to get them "just suspended" according to Zwietering's criterion.[11] The settling velocity of these particles, again in a Newtonian liquid with $\eta = 10^{-2}$ Pa·s, is roughly $v_s \approx 7$ cm/s, and the associated settling Reynolds number is $Re_{ps} \approx 5$. Their Stokes relaxation time $\tau = \rho_s {d_p}^2/18\eta$ is 5.8 ms, or 116 time steps.

As mentioned above, the liquid flow dynamics was resolved using the lattice-Boltzmann method. In its basic implementation (as used in this study), the method applies a uniform, cubic grid. The spatial resolution of the grid was such that the tank diameter, T, equals 180 grid spacings, Δ. The time step is such that the impeller revolves once in 2000 time steps. The rotation of the impeller in the static grid is represented by an immersed boundary technique, also known as the adaptive force field method.[6] The above simulation procedure (as very briefly outlined) has been extensively used (and validated against experimental data) in a number of studies on turbulent flows in mixing tanks containing Newtonian liquids.[6,12,13] The spatial resolution of $\Delta = T/180$ is sufficient to fairly accurately capture the main features of (Rushton) stirred-tank flow.[6] Higher resolutions would have been feasible and to a certain extent beneficial.[12,13] Given the significant number of flow cases to be considered in this study and the large numbers of particles in the tank, it was decided to apply this relatively modest spatial resolution of the flow simulations.

All simulations were started with a zero liquid and particle velocity field, with the particles distributed according to a uniform random distribution throughout the whole tank. The first 40 impeller revolutions of each simulation were used to study and visualize the startup behavior of the solid−liquid system. Subsequently, each simulation was continued for at least 30 impeller revolutions to collect liquid flow and solid particle motion statistics.

Results

Impressions. Clearly the presence of a yield stress has a significant impact on the flow and particle dynamics; see Figure 4. In this figure, we compare the base case with the case that has exactly the same characteristics as the base case, except for a yield stress that was set to zero. The Bingham base case shows much more viscous behavior, as witnessed from the size of the flow structures and the overall left-right symmetry. It has a significant part of the tank volume with virtually zero liquid velocity. The active part of the tank volume is usually termed the cavity. The size and shape of cavities have been investigated experimentally and numerically by a number of researchers.[14−17] For the base case, the cavity comprises approximately two-thirds of the tank volume; the cavity clearly interacts with the tank walls, which makes comparison with models that neglect such interactions[14,15] impossible. The Newtonian case is turbulent, as evidenced by the development of eddy-like small-scale structures in the liquid flow and (in the vertical cross section shown in the figure) the absence of left-right symmetry.

The distribution of particles and particle velocities (also displayed in Figure 4) reflects the observations made of the liquid flow. In the Bingham case, the particles outside the cavity hardly move. Because the impeller speed is below the just-suspended speed of the Newtonian case, there is a very high concentration of particles on and just above the tank's bottom and a clear vertical particle concentration gradient. A view of the particles through the bottom (Figure 5) once again demon-

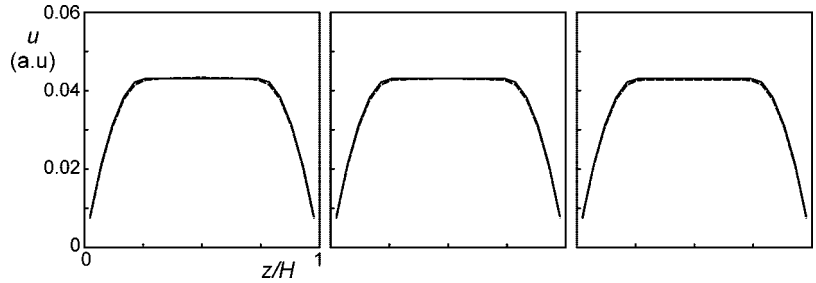

Figure 3. One-dimensional channel flow with a Bingham liquid; streamwise velocity profiles. Solid curves, analytical result; dashed curves, simulation results on a grid that has 21 lattice spacings along the channel height H. From left to right: $\eta_0/\eta = 62.5, 125, 250$.

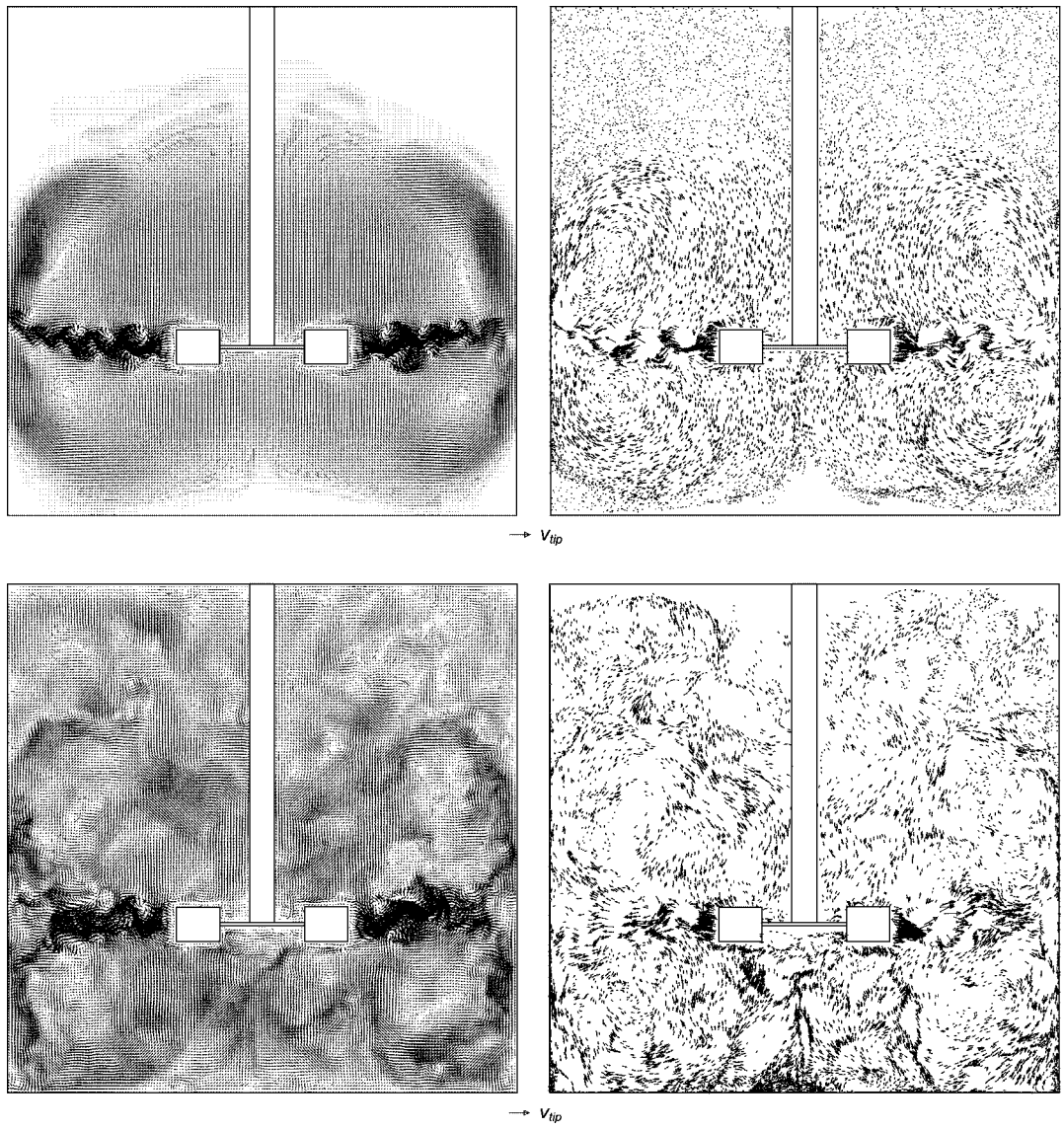

Figure 4. Snapshots from (top) the base-case simulation and (bottom) a Newtonian simulation (same as base case except with $Y = 0$). Left: liquid velocities in a vertical, midbaffle plane. Right: solid particles (and their velocity vectors) that are in a vertical, midbaffle slice with thickness $0.01T$.

strates the turbulent nature of the Newtonian case and the laminar nature of the Bingham case, with large-scale structures and symmetries for the latter. The predictions as laid down in Figure 5 (specifically for the Bingham case) are an interesting opportunity for experimental validation by means of visualizing particles through the tank bottom. As observed before, the Newtonian case has a much higher particle concentration closely above the bottom than does the Bingham case.

Cavity (Liquid-Flow Results). In Figure 6, we show velocity magnitude contours in a midbaffle plane at a series of moments after starting spinning the impeller. The formation of a cavity is visualized by plotting the contours of only the velocities larger than 1% of the impeller tip speed (in view of the usual way of defining a cavity[18] as that part of the tank with a velocity of at least $0.01v_{tip}$). We observe that the cavity has fully developed after 20 impeller revolutions. It is largely (but not perfectly) symmetric. Under the given circumstances, the cavity also is not a static phenomenon. After reaching its full size, the cavity "breathes" slowly and erratically (on a time scale of a few times the impeller revolution period; see Figure 7). Closer inspection

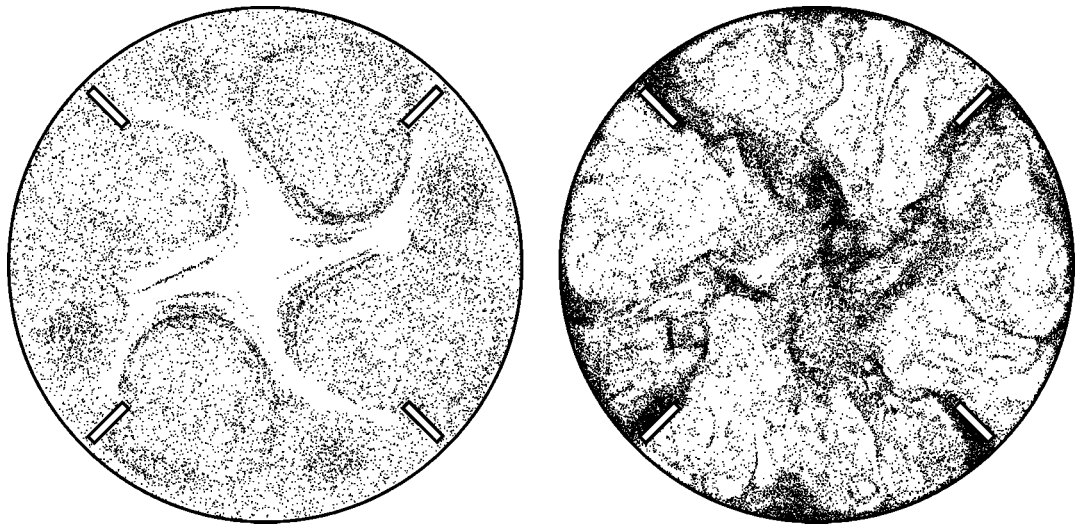

Figure 5. Snapshots of particles present in a horizontal slice through the tank with thickness $0.011T$ and center level $z = 0.02T$ above the tank bottom for the base case (left) and Newtonian case (right).

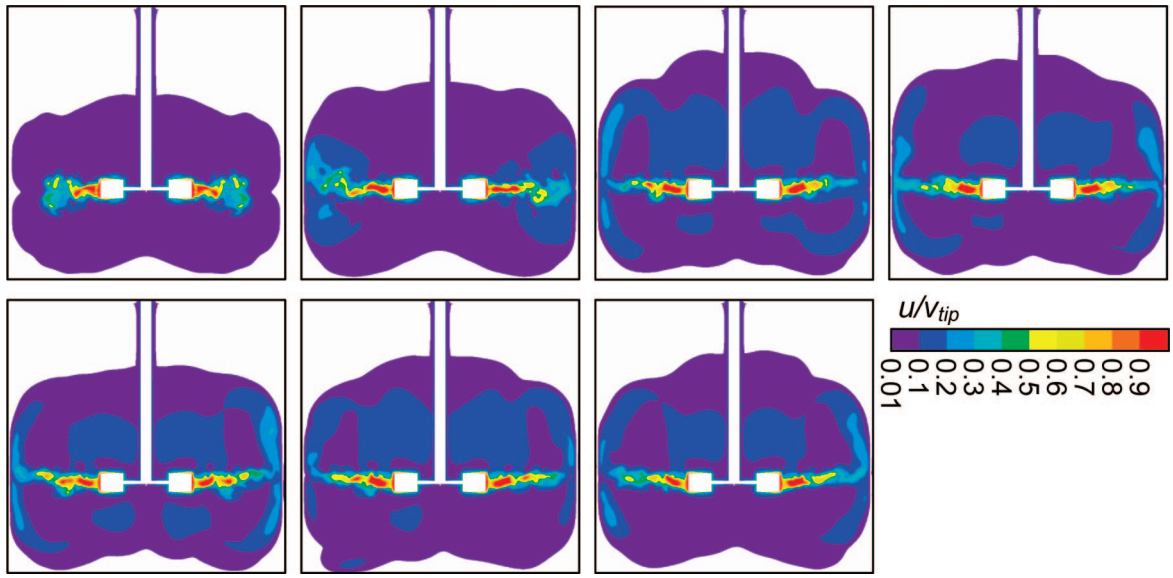

Figure 6. Snapshots of absolute velocity contours in a vertical cross section through the center of the tank between two baffles at different moments in time after startup from a zero velocity field. From left to right and from top to bottom: $tN = 1, 4, 20, 25, 30, 35, 40$. For the base case, $Re = 6 \times 10^3$ and $Y = 1.64 \times 10^{-2}$.

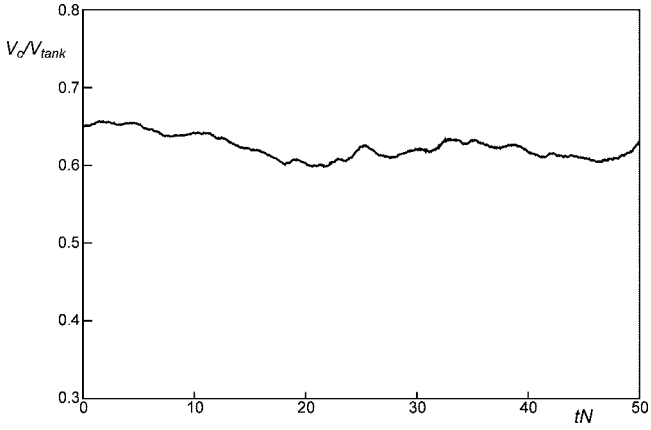

Figure 7. Cavity volume as a function of time in the base case under quasisteady conditions.

reveals that this breathing is the result of a feed-back mechanism: The smaller the cavity, the stronger the liquid stream emerging from the impeller. A strong impeller stream, however, tends to erode the edges of the cavity, making it larger and thereby weakening the strength of the impeller stream, making the cavity smaller again, and so on.

Time-averaged velocity fields are shown in Figure 8. Collection of the average data presented in this figure started 40 impeller revolutions after startup and continued over 30 impeller revolutions. The color scale of Figure 8 is the same as that of Figure 6; from now on, we will indicate the average cavity with that part of the tank volume that has an average absolute velocity higher than $0.01v_{tip}$. Figure 8 shows the impact of modeling choices on the average liquid flow field. The choice of the artificial parameter η_0 used to mimic Bingham behavior with a viscous flow solver has some impact on the liquid flow field. In the base case ($\eta_0 = 667\eta$), the average cavity volume is 64.0% of the total tank volume; if η_0 is increased to $\eta_0 = 1333\eta$, the time-averaged velocities and cavity size get slightly smaller (the latter becomes $0.629V_{tank}$). Further increasing η_0 to 2000η (results not shown in Figure 8) yields a cavity volume of

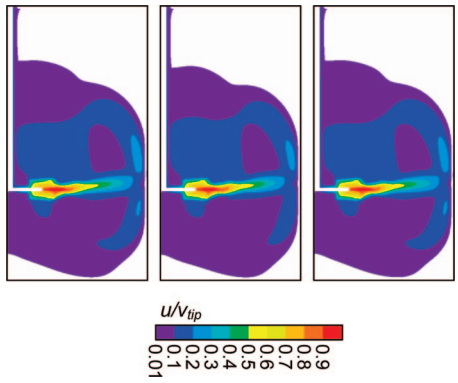

Figure 8. Average velocity magnitude field in the midbaffle plane represented with the same color scale as the snapshots of Figure 6. All three panels have $Re = 6 \times 10^3$ and $Y = 1.64 \times 10^{-2}$. Left, base case; middle, same as the base case except for η_0 (defined in Figure 2), which is twice as high; right, same as the base case except that two-way coupling between liquid and solids has been applied.

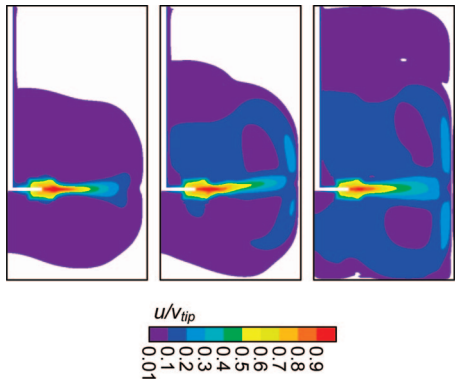

Figure 9. Average velocity magnitude field in the midbaffle plane. The middle panel is the base case with $Re = 6 \times 10^3$ and $Y = 1.64 \times 10^{-2}$. In the left panel, the impeller speed has been reduced by a factor of 2 (and thus $Re = 3 \times 10^3$ and $Y = 6.56 \times 10^{-2}$); in the right panel, the impeller speed is a factor of 2 higher (so that $Re = 12 \times 10^3$ and $Y = 0.41 \times 10^{-2}$).

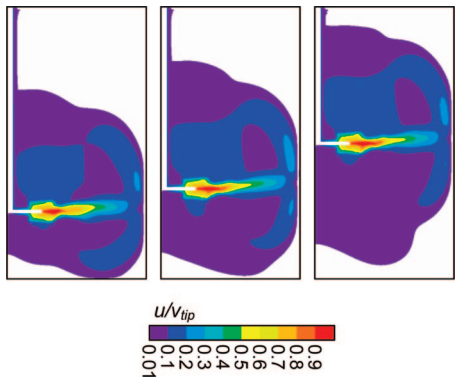

Figure 10. Average velocity magnitude field in the midbaffle plane with $Re = 6 \times 10^3$ and $Y = 1.64 \times 10^{-2}$. The center panel has the base-case impeller bottom clearance of $T/3$. The left panel has a clearance of $T/4$, and the right panel has a clearance of $T/2$.

$0.621V_{tank}$. We conclude that the flow structure and cavity shape are not very sensitive to the choice of η_0.

As explained above, the liquid flow simulations were coupled to the solid particle motion. In the default modus, particles are one-way-coupled to the liquid flow: the particles feel the presence of the liquid, but the liquid does not feel the particles. For the fairly viscous cases with modest solids loadings as studied here, one-way coupling appears to be a fair assumption:

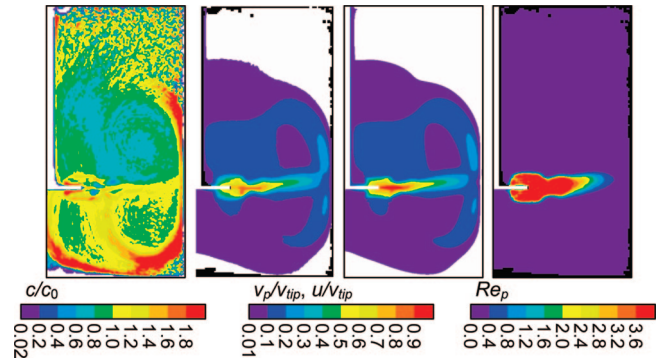

Figure 11. Solid−liquid interaction viewed in the midbaffle plane for the base case. From left to right: average particle concentration, average particle velocity, average liquid velocity, average particle Reynolds number based on the slip velocity. The black spots in the solid velocity and Re_p panels indicate that no particles were present and no average could be defined there.

In Figure 8 (right panel), results are presented that do consider two-way coupling for a situation with the base-case solids loading of 3.37% by mass. The average liquid flow field with two-way coupling is virtually the same as that with one-way coupling. Close inspection shows that the two-way-coupled cavity is a very little bit smaller ($0.638V_{tank}$) than the one-way-coupled cavity. This is within statistical uncertainty in light of the temporal fluctuations of the cavity volume (Figure 7).

Changing the impeller speed obviously has an impact on the liquid flow structure, including the size of the cavity. If the impeller speed changes for the same tank and liquid properties, both Re and Y change. Figure 9 shows contours of the absolute liquid velocity at the three impeller speeds investigated: the base case, twice the base-case impeller speed, and one-half the base-case impeller speed. At the higher speed, the active volume increases significantly, with the cavity filling almost the entire tank. It is interesting to see the subtle changes in the average inclination angle of the liquid stream emerging from the impeller. At the low impeller speed, the angle is virtually zero. This is because the cavity is so small that the flow does not reach the bottom or the top of the tank, making the flow quite symmetric with respect to the impeller level. The asymmetry is strongest for the base case, leading to a significant upward inclination of the impeller stream. For the high impeller speed, the average flow is again relatively symmetric with respect to the impeller level. The consequences of the changes in flow pattern with impeller speed for the distribution of particles in the tank will be discussed in the next section.

Finally, the influence of the impeller placement was investigated. We compared the flow induced by the impeller placed at a clearance of $T/3$ (base case), with $T/4$ and $T/2$ clearances (Figure 10). The main observation is that, at the same values of Re and Y, the $C = T/2$ placement has the largest cavity volume: $0.695V_{tank}$, $0.640V_{tank}$, and $0.570V_{tank}$ for $C = T/2$, $T/3$, and $T/4$, respectively.

Solids Concentrations and Velocities. In this section, the results regarding solid particle concentration and dynamics are presented. The solids average velocity field is almost a perfect copy of the liquid average velocity field: compare the center two panels of Figure 11. The minor differences can be explained as the effects of solids inertia. In the impeller stream close to the impeller, the solids move slightly slower than the liquid: inertia requires time to bring the solid particles up to speed. For same reason (inertia), the solid particle impeller stream extends a bit farther toward the tank wall than does the liquid stream. Inertia effects are weak though, given the modest slip

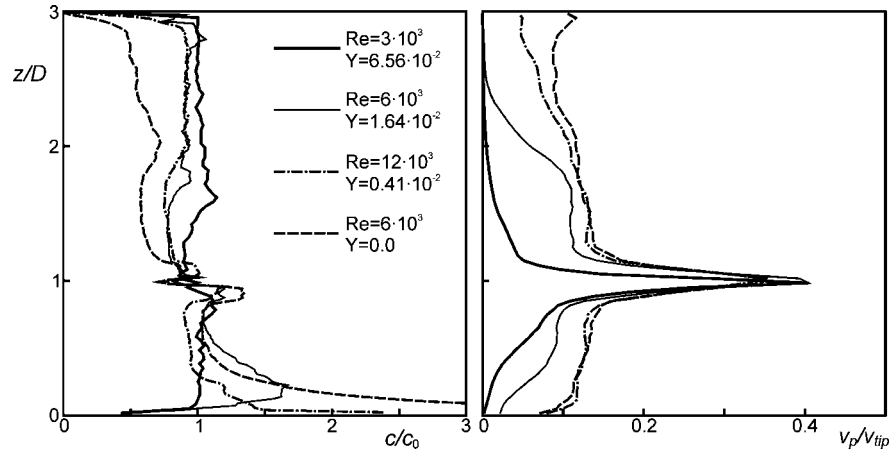

Figure 12. Vertical solids concentration (left) and velocity (right) profiles for three Bingham cases with different impeller speeds and one Newtonian simulation (having $Y = 0$ by definition).

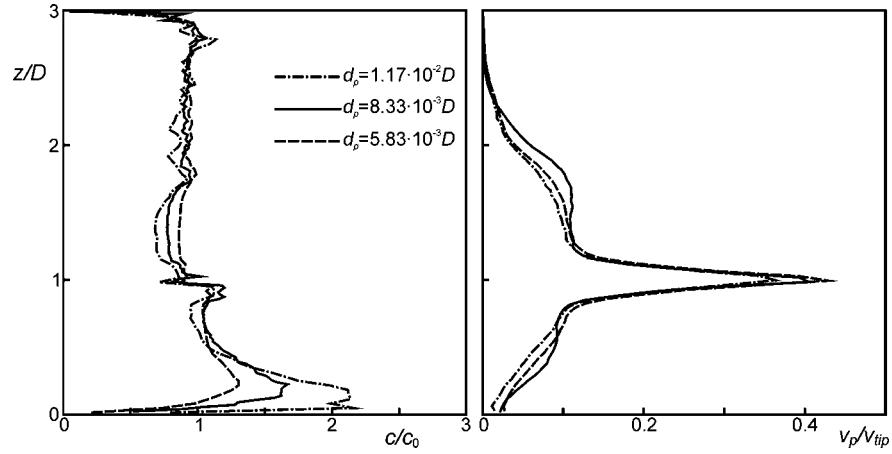

Figure 13. Vertical solids concentration (left) and velocity (right) profiles for three Bingham cases with different particle sizes but otherwise the same characteristics as the base case (including the solids mass fraction of $\phi_m = 0.0337$).

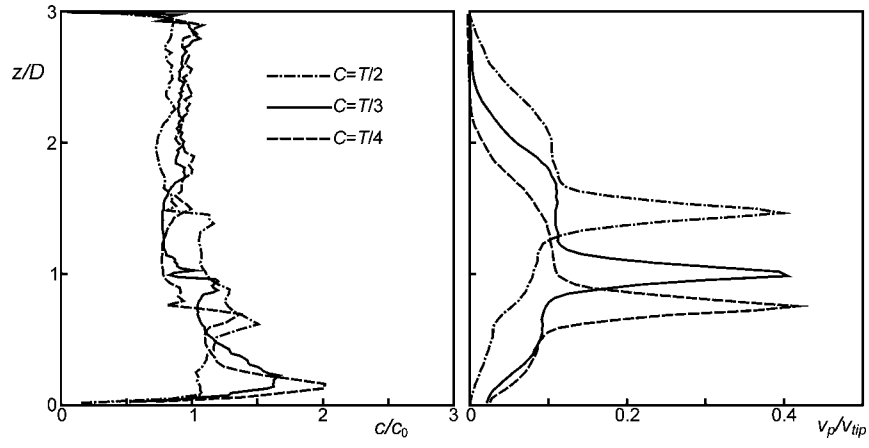

Figure 14. Vertical solids concentration (left) and velocity (right) profiles for three Bingham cases with different impeller clearances C but otherwise the same characteristics as the base case.

velocity Reynolds numbers (not getting much higher than 5) and associated Stokes numbers

$$St = \frac{\rho_s|\mathbf{u} - \mathbf{v}_p|d_p}{18\eta_a} = \frac{\rho_s}{18\rho}Re_p$$

staying well below 1. The yield-stress liquid keeps the solids distributed throughout most of the tank volume (Figure 11, left panel; the reference concentration, c_0, in this panel is the total number of particles in the tank divided by the tank volume), whereas in a Newtonian liquid loaded with the same particles and stirred at the same speed, the particles preferentially concentrate at the bottom.

In Figures 12−14, results of the time-averaged particle concentration and velocity as a function of the vertical level in the tank are presented. In Figure 12, the three cases with Bingham liquids with different impeller speeds are compared with the Newtonian case that has the same characteristics as the base case except for the yield stress. The vertical solids

concentration profiles show an interesting trend with impeller speed: at the lowest speed, the profile shows an almost uniform concentration, with the particles largely being trapped by the yield stress (only at the impeller level do particles have significant velocity). The higher the impeller speed, the more nonuniform the particle concentration (in a way, this is opposite to the effect observed with Newtonian fluids, where stronger stirring enhances uniformity). The Newtonian concentration profile is the least uniform, with a large accumulation of particles near the bottom, in agreement with the fact that the impeller speed is significantly below the just-suspended impeller speed. If we relate the vertical particle concentration profiles of the Bingham cases with the shapes of the cavities at different impeller speeds (Figure 9), the nonmonotonic behavior of the profiles at the bottom and above the impeller can be appreciated. In the bottom region, the lower two impeller speeds show similar cavity shapes and particle concentration profiles that tend to low values directly above the bottom. At the highest speed, the liquid gets mobilized down to the bottom, and the particles tend to settle, similarly to the Newtonian case. Above the impeller, the particle concentrations are virtually uniform with levels, largely slaved to the number of particles not moved to the lower regions of the tank.

Results with three different particle sizes are shown in Figure 13. These three simulations are one-way-coupled, so that the particles move around in (at least on average) the same liquid flow field. The particle size has been changed while the rest of the conditions have been kept the same, including the solids loading. Although we apply one-way coupling, solids volume fraction effects are to be expected, as particle−particle collisions are being considered. Keeping the solids loading constant is quite a computational burden for the smaller particles with a size of $5.83 \times 10^{-3}D$. We have to increase the number of particles from a little less than one million in the base case to almost three million. The vertical particle concentration and velocity results show predictable trends, with a more pronounced concentration profile for the larger particles and with the larger particles attaining less speed in the impeller outstream.

Finally, the effect of the placement of the impeller on particle behavior was investigated. Placing the impeller low limits the active volume to close above the bottom, giving the particles a chance to partly sediment and leading to a particle concentration profile that is peaked near the bottom. Shifting the impeller up homogenizes the particle concentration. Obviously, the highest particle velocities are observed at the impeller level. The larger active liquid volume for $C = T/2$ (Figure 10) is reflected in a wider particle velocity profile along the vertical direction.

Conclusions

Liquid−solid suspensions involving liquids exhibiting a yield stress have great relevance in (among many other fields) oil sands processing. Separation of the various phases and the consistency of the mixture depend critically on how mobile the solids phase is under agitation. For this reason, we performed numerical simulations of the liquid−solid flow in a laboratory-scale stirred-tank geometry.

The flow conditions were such that no turbulence model was needed to resolve the fluid flow. The fluid flow was solved with a lattice-Boltzmann scheme. The Bingham rheology was incorporated in this viscous scheme by mimicking the yield stress as a very high viscosity, η_0, at low deformation rates. The choice of η_0 was shown to be not decisive for the results as long as $\eta_0 \geq 100\eta$. Particles were tracked in the numerically determined fluid flow. Based on a detailed comparison between one-way-coupled and two-way-coupled simulations, it was concluded that one-way coupling (particles feeling the fluid flow, but the fluid flow not feeling the particles) was a reasonable assumption under the mild solid loading conditions considered in this study.

As is well-known from earlier experimental and computational studies, an active volume (cavity) is formed around the impeller in agitated Bingham liquids. Farther from the impeller, the liquid is virtually stagnant. Both the placement of the impeller in the tank and the impeller speed have significant consequences for the size and shape of the cavity. Furthermore, the cavity is not a static phenomenon. The cavity size and its flow field are coupled such that a smaller cavity results in more intense flow that tends to erode the cavity walls. This leads to a weakly unstable feedback mechanism with the cavity varying erratically in size (on the order of 10% by volume) in the course of time.

For cases such as those considered here, in which the slip velocity between the solid particles and the liquid was small, and the solids velocity field is largely a copy of the fluid flow field. Slip velocities between solid and liquid are primarily observed in the impeller stream where accelerations are such that solid particle inertia becomes appreciable. Interestingly but not surprisingly, more intense stirring leads to a less uniform distribution of particles in the tank: The apparent viscosity decreases with faster stirring, and the particles become more mobile, with gravity pulling them to the bottom of the tank where they then preferentially concentrate. In practical applications, such results (and/or the simulation procedure that was used) could guide the design of agitation systems for separating solids from yield-stress liquids.

In a more general sense, the simulation method presented here has interesting applications for guiding experimental work and process design. Extension toward more complex rheology (e.g., shear-thinning behavior) is relatively straightforward. It should be realized, however, that important issues need further research. These mainly fall in the category of microscale (sand-particle-level) phenomena and the impact that time-dependent rheology (thixotropy) would have on the results. In integrating the equations of motion of the particles, correlations for the drag in Newtonian fluids were applied. In future work, this approach could be refined by using results of experiments and simulations on spheres moving through non-Newtonian liquids.[3,19]

The thixotropy of clay suspensions potentially impacts the macroscopic (mixing-tank) level, as well as the microscopic (sand-particle) level. At the macroscale, the agitation usually is inherently time-dependent (e.g., an impeller revolving relative to a baffled tank wall as applied in this study), and as a result, an interplay between imposed (related to stirring) and inherent (in the liquid phase) time scales will develop. At the microscale, particles moving through thixotropic liquids show complex behavior[20] that could prove highly relevant for practical purposes. A meaningful integration of our understanding at the microscale into the macroscale (i.e., a multiscale approach) is an additional challenge when dealing with multiphase flows involving complex fluids.

Literature Cited

(1) Masliyah, J.; Zhou, Z. J.; Xu, Z.; Czarnecki, J.; Hamza, H. Understanding water-based bitumen extraction from Athabasca oil sands. *Can. J. Chem. Eng.* **2004**, *82*, 628.

(2) Derksen, J. J. Numerical simulation of solids suspension in a stirred tank. *AIChE J.* **2003**, *49*, 2700.

(3) Yu, Z.; Wachs, A. A fictitious domain method for dynamic simulation of particle sedimentation in Bingham fluids. *J. Non-Newtonian Fluid Mech.* **2007**, *145*, 78.

(4) Chen, S.; Doolen, G. D. Lattice Boltzmann method for fluid flows. *Annu. Rev. Fluid Mech* **1998**, *30*, 329.

(5) Succi, S. *The Lattice Boltzmann Equation for Fluid Dynamics and Beyond*; Clarondon Press: Oxford, U.K., 2001.

(6) Derksen, J.; Van den Akker, H. E. A. Large-eddy simulations on the flow driven by a Rushton turbine. *AIChE J.* **1999**, *45*, 209.

(7) Beverly, C. R.; Tanner, R. I. Numerical analysis of extrudate swell in viscoelastic materials with yield stress. *J. Rheol.* **1989**, *33*, 989.

(8) Schiller, L.; Naumann, A. Uber die grundlagenden Berechnungen bei der Schwerkraftaufbereitung. *Ver. Dtsch. Ing. Z.* **1933**, *77*, 318.

(9) Chen, M.; Kontomaris, K.; McLaughlin, J. B. Direct Numerical Simulation of Droplet Collisions in a Turbulent Channel Flow. Part I: Collision Algorithm. *Int. J. Multiphase Flow* **1998**, *24*, 1079.

(10) Crowe, C. T.; Troutt, T. R.; Chung, J. N. Numerical models for two-phase turbulent flows. *Annu. Rev. Fluid Mech.* **1996**, *28*, 11.

(11) Zwietering, Th. N. Suspending of Solid Particles in Liquid by Agitators. *Chem. Eng. Sci.* **1958**, *8*, 244.

(12) Derksen, J. Assessment of large eddy simulations for agitated flows. *Chem. Eng. Res. Des.* **2001**, *79*, 824.

(13) Hartmann, H.; Derksen, J. J.; Montavon, C.; Pearson, J.; Hamill, I. S.; Van den Akker, H. E. A. Assessment of large eddy and RANS stirred tank simulations by means of LDA. *Chem. Eng. Sci.* **2004**, *59*, 2419.

(14) Wilkens, R. J.; Miller, J. D.; Plummer, J. R.; Dietz, D. C.; Myers, K. J. New techniques for measuring and modeling cavern dimensions in a Bingham plastic fluid. *Chem. Eng. Sci.* **2005**, *60*, 5269.

(15) Amanullah, A.; Hjorth, S. A.; Nienow, A. W. A new mathematical model to predict cavern diameters in highly shear thinning, power law liquids using axial flow impellers. *Chem. Eng. Sci.* **1998**, *53*, 455.

(16) Elson, T. P.; Cheesman, D. J.; Nienow, A. W. X-ray studies of cavern sizes and mixing performance with fluids possessing a yield stress. *Chem. Eng. Sci.* **1986**, *41*, 2555.

(17) Solomon, J.; Elson, T. P.; Nienow, A. W.; Pace, G. W. Cavern sizes in agitated fluids with a yield stress. *Chem. Eng. Commun.* **1981**, *11*, 143.

(18) Adams, L. W.; Barigou, M. CFD analysis of caverns and pseudo-caverns developed during mixing of non-Newtonian fluids. *Chem. Eng. Res. Des.* **2007**, *85*, 598.

(19) Beris, A. N.; Tsamopoulos, J. A.; Armstrong, R. C.; Brown, R. A. Creeping motion of a sphere through a Bingham plastic. *J. Fluid Mech.* **1985**, *158*, 219.

(20) Ferroir, T.; Huynh, H. T.; Chateau, X.; Coussot, P. Motion of a solid object through a pasty (thixotropic) fluid. *Phys. Fluids* **2004**, *16*, 594.

Received for review August 26, 2008
Revised manuscript received November 24, 2008
Accepted December 8, 2008

IE801296Q